ACS Catalysis

Research Article

pubs.acs.org/acscatalysis

Niobium-Containing Hydroxyapatites as Amphoteric Catalysts: Synthesis, Properties, and Activity

Paolo Carniti,[†] Antonella Gervasini,*[,†,‡] Cristina Tiozzo,[§] and Matteo Guidotti[§]

[†]Dipartimento di Chimica, Università degli Studi di Milano, via Camillo Golgi, 19, I-20133 Milano, Italy

[‡]CIMaINa, Università degli Studi di Milano, via Celoria 16, I-20133 Milano, Italy

[§]CNR-Istituto di Scienze e Tecnologie Molecolari, via Camillo Golgi 19, I-20133 Milano, Italy

Supporting Information

ABSTRACT: We present here a new class of Nb-containing catalysts offering both acid and base functionalities thanks to the hydroxyapatite (HAP) structure, which acts as a host matrix for guest niobium species. Incorporation of Nb has led to samples with strengthened amphoteric properties with a prevalence of acid or basic sites depending on the synthesis procedure. Nb-containing HAP samples (12−14 wt % of Nb) have been synthesized by coprecipitation in water and in alcoholic solutions and by impregnation starting from different precursors. The intrinsic and effective acid and base properties have been measured, and a series of mass and surface characterizations have been performed to determine the Nb content, its oxidation state as well as its morphologic, structural, and electronic properties. The performances of the samples have been studied in several reactions of liquid−solid heterogeneous catalysis in batch or fixed tubular reactors working in the recirculation mode on the basis of the known catalytic features of Nb, including hydrolysis, acid-catalyzed isomerization, and selective oxidation reactions.

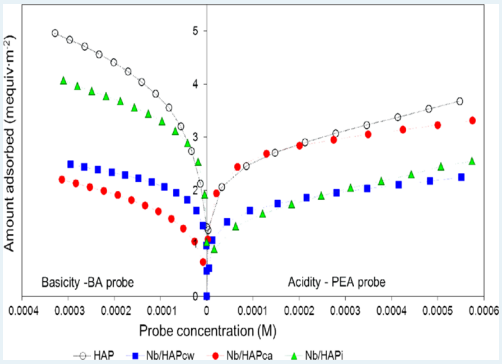

KEYWORDS: *calcium hydroxyapatite, niobium catalysts, solid acidity, solid basicity, amphoteric properties of catalysts, oxidation reactions, saccharide conversion*

INTRODUCTION

Calcium hydroxyapatites (HAPs, $Ca_{10}(PO_4)_6(OH)_2$) obtained by synthesis have been extensively used in a variety of applications, such as biomaterials, ion exchangers, adsorbents, and catalysts.[1,2] All HAP compounds present a high chemical and thermal stability and insolubility in water, properties that are useful for their use in heterogeneous catalysis.

The applications of HAP in catalysts exploit its acid−base[3] and redox[4,5] properties, which can be easily adjusted taking advantage of the flexibility of the apatite structure. With respect to the acid−base properties, HAP has the unusual feature of containing both acid sites and basic sites in a single crystal lattice. Stoichiometric HAP, characterized by a Ca/P molar ratio of 1.67, has been shown to possess a prevalence of basic sites over the acid sites, and the nonstoichiometric HAP forms (Ca/P ranging from 1.50 to 1.67) display more acid characteristics.[3,6] In general, many ionic elements and groups can be exchanged if the charge balance is maintained. For example, Ca^{2+} ions can be exchanged with divalent (Cu^{2+}, Co^{2+}, Ni^{2+}, Zn^{2+}, Mn^{2+}, Pb^{2+}, or Sr^{2+})[7−10] or trivalent (Fe^{3+}, Cr^{3+}, Al^{3+}, and La^{3+})[8,11−13] metal cations, thus giving rise to effective catalysts for various reactions. Also, the hydroxyl groups localized in the HAP tunnel can be exchanged with other types of anions, such as Cl^-, F^-, Br^-, and the phosphate groups can be substituted by anion groups, as vanadates.[14,15]

All of this evidence on the catalytic properties of the exchanged HAPs convinced us that the surface properties of these compounds can be modified and directed toward a specific catalytic use. To our best knowledge, Nb species have not been accommodated yet into the host HAP structure with the final aim of obtaining amphoteric catalysts.

Niobium inserted in or deposited onto inorganic oxide structures is an interesting catalytic species with particular acidic and redox properties,[16−20] which has been used in several selective oxidation[17,21−24] and acid-demanding reactions.[22,25] Nb-containing catalytic systems, both mixed oxide[25,26] and zeolite systems,[27,28] have shown interesting performances. In addition, the literature reports several Nb-containing crystalline solids with versatile catalytic features and well-defined structures that can be applied in oxidation,[29−33] insertion,[34] and acid-catalyzed transformations.[35,36]

One of the distinguishing feature of the Nb catalysts is the resistance to water of the isolated Nb Lewis acid sites (LAS),[28,37] which can maintain lively catalytic activity in polar and protic solvents,[38] differently from many conventional LAS-containing catalysts. The *effective* acidity in water of some

Received: September 11, 2013
Revised: December 16, 2013
Published: December 20, 2013

   dx.doi.org/10.1021/cs4010453 | ACS Catal. 2014, 4, 469−479

catalysts containing Nb has been experimentally demonstrated by various catalytic and analytical measurements,[38,39] and it has been exploited for reactions of biomass valorization realized in water.[25,40,41]

Thus, our main purpose was to assess the effect of Nb presence in/on the HAP matrix and to explore how the synthesis method of the Nb/HAP structures can affect their physical, chemical, and catalytic properties. Several liquid−solid heterogeneous reactions have been chosen as probe tests to enlighten the catalytic feature of niobium species, including hydrolysis, dehydration, acid-catalyzed isomerization, and oxidation reactions.

This study provides the first evidence that Nb/HAP samples can be successfully used as a new family of amphoteric catalysts with tunable acid−base properties.

1. EXPERIMENTAL SECTION

1.1. Catalyst Preparation. All the chemical reactants, diammonium hydrogen phosphate ($(NH_4)_2HPO_4$, VWR Prolabo AnalaR Normapur), calcium nitrate ($Ca(NO_3)_2$, Merck ACS), ammonium hydroxide ($NH_4(OH)$, Fluka, 28 wt %), and niobium chloride ($NbCl_5$, Aldrich, 99%) were reagent-grade chemicals, and they have been used without any further purification. Ammonium niobium oxalate complex, $(NH_4)NbO(C_2O_4)_2{\cdot}nH_2O$ (ANBO), was kindly supplied from Companhia Brasileira de Metallurgia e Mineração (CBMM).

Stoichiometric calcium hydroxyapatite, $Ca_{10}(PO_4)_6(OH)_2$, with a Ca/P molar ratio of 1.67 was synthesized by the coprecipitation method, adopting the procedure reported by C. Lamonier et al.[3]

Niobium was introduced during the HAP synthesis using ammonium niobium oxalate, ANBO, or niobium chloride as Nb precursors by the coprecipitation method (*one-step* synthesis) or by the Nb deposition by impregnation of presynthesized HAP sample. An amount of about 12−14 wt % of Nb was introduced in the final sample.

Nb/HAPcw was synthesized using aqueous solutions of calcium nitrate (0.372 M in 100 mL) and ammonium niobium oxalate complex (0.083 M in 100 mL) simultaneously pumped at a constant rate (0.55 mL·min^{-1}) into an aqueous solution of diammonium hydrogen phosphate (0.12 M in 250 mL) while stirring and maintained at 90 °C under nitrogen atmosphere. Then, basification of the solution at pH = 10, filtration, washing, aging of precipitate, and solid drying (50 °C in vacuo) and calcination (600 °C for 4 h) were carried out.

For the Nb/HAPca synthesis, an ethanol solution of niobium chloride (0.083 M in 100 mL of ethanol) and a water solution of calcium nitrate (0.3725 M in 100 mL) were simultaneously pumped at constant rate (0.55 mL·min^{-1}) into a hydroalcoholic solution of diammonium hydrogen phosphate (0.12 M in 0.25 mL of 1:1 ethanol−water solution), while they were stirred and maintained at 70 °C under nitrogen atmosphere. The successive operations of basification of the solution, precipitate filtration, washing, aging, and drying and calcination of the solid were carried out as referred to above.

The sample labeled Nb/HAPi was prepared by impregnation of ammonium niobium oxalate of a presynthesized HAP sample. A weighted amount (5 g) of dried HAP was added to ammonium niobium oxalate water solution (0.16 M in 50 mL), and they were stirred and maintained at 30 °C for about 15 h. Then, water was removed by evaporation at 50 °C under vacuum. Drying and calcination of the solid were performed as reported above.

1.2. Catalyst Characterization. Inductively coupled plasma (ICP) measurements were determined by ICP-OES (plasma optic emission spectrometer, Horiba JOBIN YVON) after solid digestion in acid mixtures ($HClO_4$ + HNO_3 + HF) followed by evaporation and new dissolution in HNO_3.

Thermogravimetric analysis (TGA) was performed on both dried and calcined samples by using a TGA analyzer from Perkin-Elmer (TGA7) in the temperature interval from 50 to 800 °C under flowing air with a ramp of 10 °C min^{-1}.

BET specific surface area ($m^2{\cdot}g^{-1}$), specific pore volume ($cm^3{\cdot}g^{-1}$), and BJH pore size distribution of the sample were determined from N_2 adsorption and desorption isotherms measured at liquid nitrogen temperature with an automatic surface area analyzer (Sorptomatic 1900 instrument). Prior to the measurement, the sample (≈100 mg), crushed and sieved as 0.250−0.354 mm particles, was thermally activated at 350 °C for 16 h under vacuum.

X-ray diffraction (XRD) of the powder samples was carried out by a Philips PW1710 vertical goniometer diffractometer using Ni-filtered CuKα radiation (λ = 1.54178 Å).

Scanning electron micrographs (SEM) were collected by a LEO-1430 coupled with an energy-dispersive X-ray spectroscopy (EDX) working with an accelerating voltage of 20 kV.

Transmission electron micrographs were collected on a Zeiss LIBRA 200FE analytical HR-TEM microscope, equipped with 200 kV FEG, in-column second-generation omega filter for energy selective spectroscopy (EELS) and for imaging (ESI), HAADF STEM facility and EDS probe for chemical analysis. UV−vis diffuse reflectance spectroscopy (UV−vis-DRS) measurements were performed on fine powder samples put in a cell with optical quartz walls of a Perkin-Elmer Lambda 35 instrument equipped with a Labsphere RSA-PE-20 integration sphere and Spectralon as reference material.

X-ray photoelectron spectroscopy (XPS) analyses were performed using a Kratos Analytical Axis Ultra DLD spectrometer with a monochromatic Al Kα (hν = 1486.6 eV) radiation source operated at 15 kV and 15 mA. The binding energy (BE) was calibrated on the basis of the line position of C 1s (285 eV). CasaXPS processing software was used to estimate the relative abundance of the different species and to deconvolute the photopeaks.

The acidity and basicity measurements of the samples in liquid by using 2-phenylethylamine (PEA) as basic probe and benzoic acid (BA) as acidic probe were carried out in cyclohexane for the *intrinsic* acidity (I.A.) and *intrinsic* basicity (I.B.), respectively, and in water for the *effective* acidity (E.A.) determination (cyclohexane and water). The samples were thermally activated at 350 °C for 16 h under air flow (8 mL·min^{-1}). A recirculation chromatographic line (HPLC) comprising a pump (Waters 515) and a monochromatic UV detector (Waters, model 2487, λ = 254 nm) was used as described in the Supporting Information (SI) and refs 41 and 42. Previous tests of PEA and BA adsorption showed that both probes are adsorbed a negligible amount on samples without any acid and basic sites (sand sample, Fluka). In addition, calibration tests by PEA and BA adsorption on acidic and basic resins, Amberlite 200 and AmberlystTM A21, respectively, (Carlo Erba and Dow) were performed with a certified amount of acid and basic sites.

1.3. Catalytic Activity. *1.3.1. α-Pinene Oxide Isomerization.* Tests of the catalytic isomerization of (−)-α-pinene

dx.doi.org/10.1021/cs4010453 | ACS Catal. 2014, 4, 469−479

Table 1. Composition of the Nb/HAP Samples

sample	elemental composition used for synthesis					actual elemental composition[c]				
	wt %			atomic ratio		wt %			atomic ratio	
	Nb	Ca	P	Nb/P	Ca/P	Nb	Ca	P	Nb/P	Ca/P
HAP[a]		40.0	18.5		1.67		37.84	18.4		1.59
Nb/HAP_{CW}	14.2	27.7	17.2	0.28	1.25	9.7	30.2	13.84	0.23	1.69
Nb/HAP_{CA}	14.2	27.7	17.2	0.28	1.25	13.1	26.5	16.4	0.26	1.25
Nb/HAP_i[b]	12.1			0.26	1.67	7.7	31.7	15.2	0.17	1.61

[a]Chemical formula considered for the preparation: $Ca_{10}(PO_4)_6(OH)_2$. [b]Prepared starting from finite HAP powder. [c]Measured by ICP.

oxide (100 mg; 0.66 mmol; 97%, Aldrich) was performed in liquid phase in a glass batch reactor (stirring rate of 1000 rpm) at room temperature using toluene as solvent (8 mL; puriss., Riedel-de-Haën), previously dried on molecular sieves (Siliporite, 3 Å). The solid catalyst (35 mg) was pretreated at 110 °C for 3 h in vacuum. The reaction was performed for 6 h, and samples were taken at regular intervals. Reaction products were determined by GC analysis (HP5890; HP-5 column, 30 m × 0.25 mm; FID or MS detectors, head pressure 160 kPa; mesitylene internal standard). Standard deviation was ± 2% and ± 3% in conversion and selectivity values, respectively.

1.3.2. Activity with Sugars in Aqueous Solvent. Sucrose, D-(−) fructose, and D-(−) glucose (RPE, Carlo Erba) were used as substrates and standards for the various analyses.

The reaction test of hydrolysis of sucrose was performed in water with the powder catalyst put in a fixed catalytic bed reactor working in a total recirculation reaction mode at atmospheric pressure, as detailedly described in refs 42 and 43 and in the SI. The reaction solution was continuously circulated (3 mL·min^{-1}) through the catalyst (0.5 g, 0.250−0.354 mm particles).

The catalytic test of glucose isomerization was carried out in water in a total recirculation reaction line equipped with a HPLC pump (Merck-Hitachi L6200 Intelligent Pump), stainless steel preheater, and fixed-bed tubular flow reactor (17 cm long, 0.5 cm internal diameter).[40,42] The initial aqueous glucose concentration (≈0.55 M) was continuously circulated (3 mL·min^{-1}) through the catalyst (3 mL·min^{-1}) at constant contact time (≈0.17 min·g·mL^{-1}). The reaction was studied for a total of 8 h. A sample (typically 1 mL) was withdrawn from the reservoir every 2 h of reaction and analyzed.

The products were analyzed by HPLC, which was assembled with an injector (Waters U6K), a pump (Waters 510), a heater (Waters CHM) for the column, and a refractive index detector (Waters 410). A SugarPak-I column (Waters) operating at 90 °C and eluted with a solution of Ca-EDTA 10^{-4} M in water (0.5 mL min^{-1}) was used.

1.3.3. Oxidation Catalytic Activity. The cyclo-octene epoxidation reaction was carried out in the fixed catalytic bed reactor working in a total recirculation reaction line at atmospheric pressure, as described above. The powder catalyst (0.6 g with 0.250−0.354 mm particles) was thermostatted at 55 ± 0.1 °C, and the feeding solution was put in the reservoir containing the cyclo-octene (0.45 M) plus H_2O_2 (0.45 M) in methanol thermostatted at 17 °C. The solution volume in the reservoir was 100 mL. The reaction solution was continuously circulated (3 mL·min^{-1}) through the catalyst. The reaction was studied for a total of 10 h. At every hour, a sample (typically 1 mL) was withdrawn from the reservoir and analyzed.

The epoxidation tests on (*R*)-(+)-limonene (97% Aldrich; 98% e.e.) were carried out in a glass batch reactor (90 °C, 800 rpm magnetic stirring) under inert atmosphere. All the samples were pretreated in vacuum at 120 °C and cooled to room temperature under vacuum prior to use. Acetonitrile (Aldrich, HPLC grade) was used as solvent. Aqueous hydrogen peroxide (H_2O_2; 50% Aldrich) was used as oxidant agent, with an oxidant to substrate molar ratio of 2:1. The total volume of the mixture was 5 mL. Samples were analyzed by GC chromatography (Agilent 6890 Series; HP-5 column, 30 m × 0.25 mm; FID or MS detector). Neither significant autoxidation nor support-catalyzed contributions to epoxidation were recorded with any sample, limonene conversion being about 10% with no remarkable epoxide formation. After all tests, the presence of residual hydrogen peroxide was checked and confirmed by iodometric assays.

In the tests of catalyst recovery, the solid was separated by filtration and thoroughly washed with fresh acetonitrile and then with methanol (Fluka, HPLC grade). The filtered solid was dried at 100 °C.

2. RESULTS AND DISCUSSION

2.1. Preparation and Characteristics. The same sequence of unit operations has been followed for the synthesis of HAP and of Nb/HAPcw (by using aqueous ANBO precursor) and Nb/HAPca (by using ethanolic NBE precursor). The unripe solids were dried and calcined to obtain the final samples. The other sample, Nb/HAPi, was prepared by ANBO deposition on presynthesized HAP by a conventional impregnation procedure.

The elemental amounts used for the synthesis and Ca/P and Nb/P ratios of all the prepared samples are presented in Table 1. Niobium-free HAP was synthesized with the Ca/P atomic ratio of 1.67, in accordance with the stoichiometric hydroxyapatite ($Ca_{10}(PO_4)_6(OH)_2$) by coprecipitation. For the Nb/HAP samples prepared by coprecipitation, in the presence of aqueous ANBO solution or of ethanolic solution of niobium chloride, an amount of Nb around 14 wt % was introduced, leading to theoretical Nb/P and Ca/P ratios of 0.28 and 1.25, respectively. The impregnated sample, Nb/HAPi, was prepared using the niobium-free HAP powder as support and deposited an amount of ≈12 wt % of Nb on it by classical wet impregnation. For HAP, the measured Ca/P ratio was lower than that expected, indicating that a Ca-deficient hydroxyapatite was formed with formation of cationic vacancies.[7] Important differences were found between Nb/HAPcw and Nb/HAPca samples: a higher Nb amount was effectively introduced in Nb/HAPca than in Nb/HAPcw, the higher amount of Nb caused the lowering of the Ca/P ratio (Ca/P of 1.25 and 1.69 for Nb/HAPca and Nb/HAPcw, respectively), with an influence on the acidity properties of these two samples (see section 2.2, Surface Acid and Base Properties). The real Nb concentration in Nb/HAPi was much lower than the nominal one; the amount of Nb

dx.doi.org/10.1021/cs4010453 | ACS Catal. 2014, 4, 469−479

not present on the HAP surface likely has segregated as a separate NbO_x phase.

TGA analyses revealed that Nb/HAPcw and Nb/HAPi, prepared from ANBO, decomposed in three steps, about at 170, 250, and 700 °C. In addition, an evident mass loss was observed at 450 °C that was due to water removal from phosphate groups of the HAP structure in interaction with Nb. Nb/HAPca, prepared from the niobium chloride precursor, showed the mass loss at 450 °C along with a broad mass diminution in the 100−200 °C interval, associated with water and ethanol removal. The thermograms of all the samples after calcination no longer presented defined peaks of mass loss; only a light mass decrease (1−2 wt %) was observed at temperatures around 700 °C (Figure S.1, SI).

The crystalline structure of niobium-free HAP and Nb/HAP samples was studied by XRD analysis. It is known that low crystallinity HAP particles have to be calcined to improve thermal and chemical stability.[43,44] All the samples exhibit diffraction lines corresponding to the typical hydroxyapatite structure (point group $P63/m$, JCPDS 01-086-0740), and the poorer crystallization of the Nb/HAP samples in comparison with bare HAP is clearly showed in Figure 1. HAP and Nb/

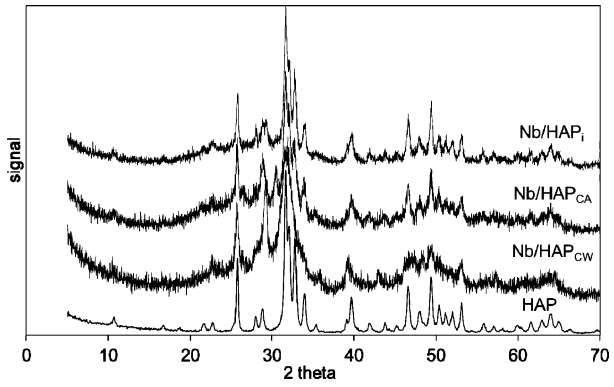

Figure 1. XRD comparative patterns of all the studied samples.

HAP present the hexagonal system made of compact assemblage of Ca^{2+} ions and tetrahedral PO_4^{3-} groups delimiting the typical unconnected channels.[7] Additional diffraction lines were not observed in the samples containing niobium, indicating the absence of Nb-separate phases in all the Nb-containing samples. Unfortunately, due to the poor crystalline feature of Nb/HAPcw and Nb/HAPca samples, it was not possible to determine whether $(NbO)^{3+}$ species had been introduced in the apatite structure by the determination of the unit-cell parameter values. Nevertheless, due to the large ionic radius of $(NbO)^{3+}$, the accommodation of the guest ions in the apatite channels cannot be excluded.

The morphology of the HAP and Nb/HAP samples was studied by direct observation of the surface images collected by SEM-EDX. The powders consist of agglomerates of individual particles with platelet-like morphology and 10−20 μm dimension, covered by a layer of small particles with the laminar-plate structure (Figure S.2, SI). The presence of Nb makes the surface of the samples smoother, denser particles have little protuberances at the surface layers transformed to microsheets. EDX-microanalysis confirmed the trend in metal content, as observed from ICP analysis. The measured Nb content was 16.8, 19.7, and 14.3 wt % for Nb/HAPcw, Nb/HAPca, and Nb/HAPi, respectively. By comparing EDX and ICP values, niobium seems to be mainly located in the first surface layers of the samples. This is particularly evident for Nb/HAPi, as expected, since niobium has been deposited by impregnation onto the HAP surface. HR-TEM analysis on the Nb/HAPca sample revealed the presence of even crystalline aggregates. At the HR-TEM level, at nanometric scale, a homogeneous distribution of Nb, Ca, and P atoms was observed. This is consistent with the formation of a definite unique structure with no evident segregation of different phases (EDX elemental mapping images in Figure S.3, SI)

The FT-IR spectra of all the samples confirmed the formation of an apatite phase with the observation of several fundamental vibration modes of PO_4^{3-} groups.[45] The Nb/HAP samples in comparison with niobium-free HAP showed a strong decrease of the intensity of ν(OH) stretching band at 3570 cm^{-1} (lattice OH− ions) and of the O−H− deformation mode at 630 cm^{-1} (Figure S.4, SI). Such a decrease is consistent with the substitution of Ca^{2+} by $(NbO)^{3+}$, which provokes the elimination of protons from the OH hydroxyls located in the apatite tunnels to counterbalance the electron excess due to the new guest species.[12,46]

The textural results of all the samples are given in Table 2. The HAP specific surface area (S_{BET}) is 43 $m^2 \cdot g^{-1}$ with low porosity. The isotherm belongs to IV type with little, but visible, hysteresis between the adsorption and desorption isotherms (Figure 2). Accordingly, a broad pore size population, with two maxima centered around 18 and 30 nm of pore diameter, was observed. The deposition of Nb on HAP (Nb/HAPi) caused a shift of the two main pore size populations with respect to HAP (Figure 2D). The coprecipitated Nb/HAP samples showed more important porosimetric differences. The Nb/HAPcw sample has a specific surface area twice higher than HAP and a more defined pore size distribution profile centered at 17 nm of size (Figure 2B). The Nb/HAPca sample has a lower surface area than Nb/HAPcw, with several distinct pore populations of different sizes (Figure 2C). This could be due to the higher amount of Nb introduced in the apatite structure, as confirmed by ICP analyses.

The diffuse reflectance UV−vis spectra of HAP consists of one broad low-intensity band located around 200 nm which can be ascribed to charge transfer $O^{2-} \rightarrow Ca^{2+}$. Following the addition of Nb, new intense LMCT (ligand-to-metal charge-transfer $O^{2-} \rightarrow Nb^{5+}$) bands appeared in the UV region (Figure S.5, SI), but it was impossible to discriminate between the contribution of tetrahedral (230 nm) or five- and six-

Table 2. Morphologic and Structural Properties of the Samples

sample	BET surface ($m^2 \cdot g^{-1}$)	pore volume ($cm^3 \cdot g^{-1}$)	pore radius (nm)
HAP	42.7	0.24	9; 15
Nb/HAP$_{CW}$	98.5	0.20	8.5
Nb/HAP$_{CA}$	55.0	0.19	6.5; 11; 15
Nb/HAP$_i$	47.7	0.21	11; 20

dx.doi.org/10.1021/cs4010453 | ACS Catal. 2014, 4, 469−479

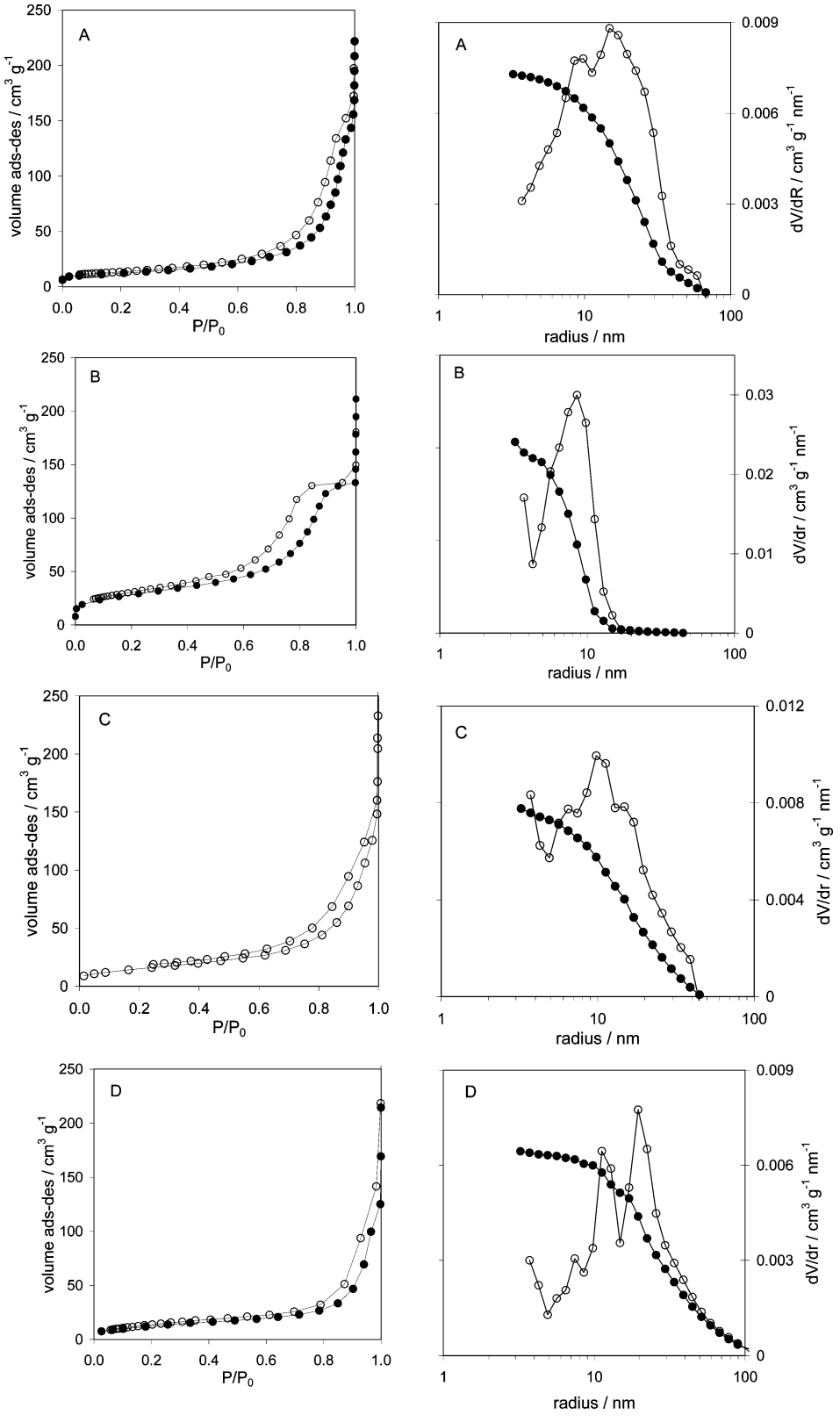

Figure 2. Isotherms of N_2 adsorption/desorption collected at −196 °C (left side) and cumulative pore volume and pore volume distribution as a function of pore radius (right side) of all the studied samples: HAP (A), Nb/HAP_{CW} (B), Nb/HAP_{CA} (C), Nb/HAPi (D).

coordinated Nb species (250 nm).[25,47] Interestingly, no band has been observed at 320 nm, confirming the absence of niobia (formed as segregated phase) in small nanodomains.[47]

Some information on the presence of Nb on the sample surface has been collected by XPS analysis. The values of Nb 3d binding energy and the shape of the peaks for all the samples are typical for niobium with a formal oxidation state of +5 ($3d_{5/2}$, values of 207.5−208.0 eV and $3d_{3/2}$, values of 210.2−201.7 eV). In Figure 3 are reported the typical doublets (Nb 3d photopeaks) observed in the 195−220 eV interval of binding

dx.doi.org/10.1021/cs4010453 | ACS Catal. 2014, 4, 469−479

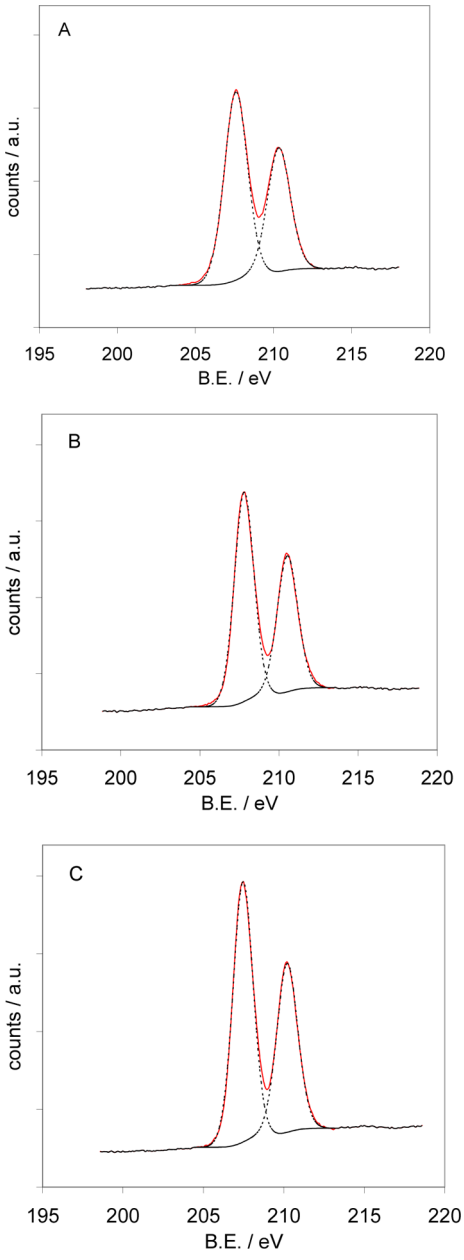

Figure 3. XPS measurements: region of Nb 3d bands of Nb/HAP_{CW} (A), Nb/HAP_{CA} (B), Nb/HAP_{i} (C).

energy for Nb/HAPcw, Nb/HAPca, and Nb/HAPi. It is known that it is possible to derive information on Nb dispersion from a close inspection of the Nb 3d photopeak broadening.[48] An increase in the values of the full width at half-maximum (fwhm) of Nb $3d_{5/2}$ and a reduction in the Nb 3d valley between the 5/2 and 3/2 components indicates the presence of well-dispersed surface Nb species, as reported by Dragone et al.[49] and already observed by some of us.[25] Both the effects are clearly observed for Nb/HAPcw (fwhm of 1.75 and 1.46 eV for Nb/HAPcw and the two Nb/HAPca and Nb/HAPi samples) and are in agreement with a better dispersion of Nb in the Nb/HAPcw sample than in the other Nb-containing samples.

2.2. Surface Acid and Base Properties. The amphoteric properties of HAP have been already showed by several groups and exploited for catalytic purposes (Scheme S.1. displays the acid and base functionalities of the HAP matrix).[3,4,6] The presence of guest ions in the HAP matrix can change the ratio between acid and basic sites of the sample, thus influencing its catalytic performance. To our best knowledge, no information about the acidity properties of hydroxyapatite hosting niobium species has been reported until now.

The Nb/HAP samples have been investigated by measuring the adsorption properties of basic (phenylethylamine, PEA) and acid (benzoic acid, BA) probe molecules in an adsorption reaction line previously reported.[41] The measurements were performed in two different liquids: an aprotic/apolar solvent, cyclohexane, and a protic/polar one, water, in order to collect information on the *intrinsic* and *effective* acidity, respectively.[25,41,50] Nb-containing catalysts are known to possess water-tolerant properties, that is, the ability to maintain lively acid properties in water and other polar and protic liquids.[37,39,40,42,51]

Figure 4 shows all the obtained results of the *intrinsic* acidity (I.A.) and *intrinsic* basicity (I.B.) for HAP and the three samples containing Nb, collected in cyclohexane. On the right side of Figure 4 are reported the first and the second isotherms of PEA adsorption and on the left side the first and the second isotherms of BA adsorption, which are related with the acidity and basicity properties of the samples, respectively. The determination of the total amount of acid(base) sites has been made from the first run isotherm (Figure S.6, SI).

As expected, HAP shows a higher amount of intrinsic basic sites than acid sites with a ratio between acid and basic sites (I.A./I.B.) of 0.71 (Table 3). The situation changed when Nb was presented into the HAP matrix, although a common-trend behavior could not be observed. The amount of acid sites increased for Nb/HAPcw and Nb/HAPca and deeply decreased for Nb/HAPi, in comparison with Nb-free HAP.

With regard to basicity, a different situation was observed. Nb/HAPcw and Nb/HAPi have a similar amount of basic sites compared to HAP, while Nb/HAPca showed half of the basic sites compared to HAP. Therefore, for the Nb/HAP samples, the ratio between the acid and basic sites was observed to shift from that of HAP; a higher value for Nb/HAPcw and, in particular, for Nb/HAPca, and a lower value for Nb/HAPi have been determined (Table 3). The lack of of acid sites on Nb/HAPi was unexpected. Nb/HAPi has a similar amount of basic sites than HAP (0.144 vs 0.155 $mmol \cdot g^{-1}$, respectively), but it has a much lower content of acid sites (0.070 vs 0.110 $mmol \cdot g^{-1}$, respectively). The amphoteric properties of all the samples (although with a somehow more marked acid or basic character) indicate that Nb was accommodated in/on different sites of HAP as a function of the preparation mode.

The influence on the acid−base site strength of the samples has been observed also, as it can be seen by comparing the isotherms of the first and second runs of PEA and BA adsorption (Table 3 and Figure 4). From the two-runs isotherms, the percentage of the strong acid sites could be calculated. The strong acid sites are 60% of the total acid sites of HAP and Nb/HAPcw, while they increase up to 80% for Nb/HAPca and deeply decrease for Nb/HAPi down to about 4%. In fact, the isotherms of the first and second runs of the PEA adsorption are very distant from each other for Nb/HAPca, and they are very close for Nb/HAPi (Figure 4C,D, right side). With respect to the basic strength of the sites, only Nb/HAPca shows an important decrease of the amount of strong basic sites (only 19%) of the total ones, while for all the other samples, the strong basic sites are around 50−59% of the total basic sites possessed (Table 3 and Figure 4, left side).

dx.doi.org/10.1021/cs4010453 | ACS Catal. 2014, 4, 469−479

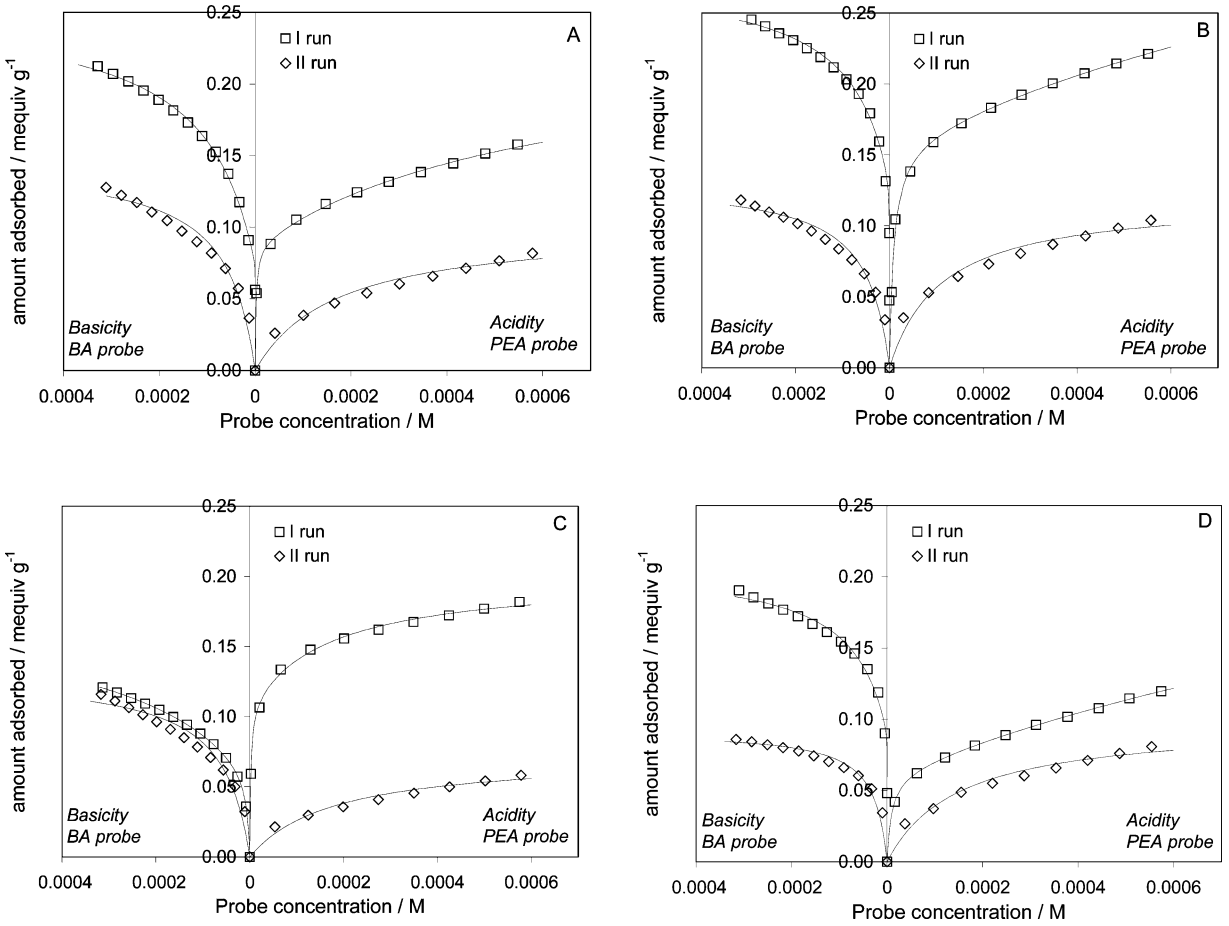

Figure 4. *Intrinsic* acidity (I.A.) and *intrinsic* basicity (I.B.) measurements of HAP and Nb−HAP samples: isotherms of 2-phenyl-ethylamine (PEA) adsorption, for acidity (right side), and of benzoic acid (BA) adsorption, for basicity (left side), in cyclohexane at 30 °C on HAP (A), Nb/HAP_{CW} (B), Nb/HAP_{CA} (C), Nb/HAi (D) (1st run was carried and on fresh sample and 2nd run after flushing the PEA(BA) saturated sample with pure solvent for 45 min).

Table 3. Surface Acidity and Basicity of HAP and Nb/HAP Samples Determined by Adsorption of Basic (2-Phenyl-Ethylamine, PEA) and Acidic (Benzoic Acid, BA) Probes[a]

sample	intrinsic acid sites (I.A.)[b] (mmol g^{-1})	intrinsic basic sites (I.B.)[b] (mmol·g^{-1})	I.A./I.B.[c] ratio	effective acid sites (E.A.)[b] (mmol·g^{-1})
HAP	0.110 (62%)[d]	0.155 (50%)[d]	0.71	0.019
Nb/HAP_{CW}	0.164 (62%)	0.196 (59%)	0.84	0.013
Nb/HAP_{CA}	0.147 (80%)	0.085 (19%)	1.73	0.029
Nb/HAP_{i}	0.070 (4.3%)	0.144 (53%)	0.49	0.019

[a]Adsorption temperature, 30 °C; solvent, cyclohexane for I.A. and I.B. measurements, water for E.A. measurements. [b]Determined at the intersection point between the straight line of the low-concentration part of the adsorption isotherm with the asymptotic part of the isotherm (Figure S.5, SI). [c]Calculated from the relevant values in the 2nd and 3rd columns. [d]Percent amount of strong acid and basic sites, determined by subtracting the second from the first isotherm of PEA or BA probe adsorption, respectively.

In summary, the rather balanced population of acid and base sites shown by HAP (I.A./I.B. = 0.71) was maintained for the sample prepared by coprecipitation in aqueous solution, Nb/HAPcw (I.A./I.B. = 0.84), with an increase in both acid and base sites, which was due to the presence of Nb and to the larger surface area of this sample in comparison with HAP. The sample prepared by coprecipitation in alcoholic solution, Nb/HAPca, had a higher amount of acid sites than basic sites; the amount of acid sites were higher than those of HAP, due to the presence of Nb. The addition of the guest Nb species to HAP by impregnation led to a sample with a prevalent basic character (Nb/HAPi with I.A./I.B. = 0.49); likely, Nb was mainly accommodated on the acid functionality of HAP, thus leaving behind the basic sites of the HAP matrix.

Effective acid properties of both HAP and Nb−HAP samples were determined in water, and the results obtained are shown in Table 3 and Figure 5. The PEA adsorption isotherms in water on all the samples (HAP and Nb/HAP) do not have a clear Langmuir-type shape, indicating low acid strength of the sites. In water, a far lower amount of effective acid sites (E.A.) than those measured in cyclohexane (I.A.) have been determined in any case. In water, Nb/HAPca showed the highest amount of effective acid sites. For the Nb/HAP samples, the measurement of the effective basicity in water has been performed, but no confident result has been determined due to the extremely weak basic strength of the sites, which are not able to manifest the basic property in water, a highly polar and protic liquid.

dx.doi.org/10.1021/cs4010453 | ACS Catal. 2014, 4, 469−479

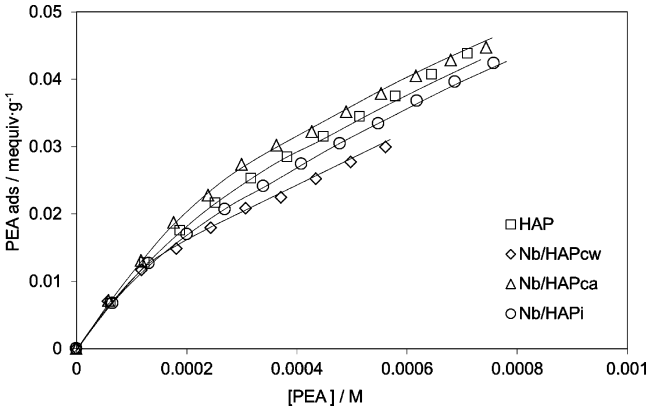

Figure 5. Effective acidity (E.A.) measurements: isotherms of 2-phenyl-ethylamine (PEA) adsorption in water on HAP and Nb/HAP samples.

2.3. Catalytic Activity. The acid character of HAP and Nb-containing HAP samples was evaluated using the catalytic rearrangement of α-pinene oxide in liquid phase, under batch conditions, as a model test reaction (Scheme 1). In the presence of acid sites, α-pinene oxide (**1**) typically isomerizes into a series of different compounds: campholenic aldehyde (**2**), carveol (**3**), pinocarveol (**4**), and pinocamphone (**5**), along with other minor compounds. The strength and the nature of the acid sites (either Lewis or Brønsted centers) have a direct influence on the quality and the distribution of products formed. Indeed, it is largely reported that the use of mild Lewis acid sites favors the production of **2** with, as main side-products, **4** and **5**, while Brønsted acid sites enhance the formation of **3**, together with the main product **2**.[52−55]

All the materials, HAP and Nb/HAP, showed a rather low activity with respect to other heterogeneous acid materials (Table 4). In fact, at 90 °C, the isomerization reaction is not complete even after 24 h. On the contrary, for the sake of comparison, a strong Brønsted acid catalyst, such as a protonic synthetic saponite clay, and a Na-exchanged saponite clay have shown, under fully comparable conditions, total (>98%) and ≈50% conversion of **1**, respectively, at room temperature, in only 5 min.[56] In particular, the catalytic activity follows this trend: Nb/HAPca > Nb/HAPi ≈ Nb/HAPcw > HAP. The highest activity for Nb/HAPca is consistent with the highest amount of effective acid sites, as reported in Table 4. The isomerization of α-pinene oxide indeed can occur on either Lewis or Brønsted acid sites, and it is roughly proportional to the total amount of acid sites on the catalyst. With regard to the selectivity, the formation of **3** was particularly remarkable over Nb/HAPca, and this reveals the presence of some active Brønsted acid sites, although not very strong, at the catalyst surface. At the same time, however, **2** and **5** were the two major

Table 4. Catalytic Performance of HAP and Nb−HAP Materials in Liquid-Phase Isomerization of α-Pinene Oxide[a]

		selectivity[c] (%)				
sample	conversion[b] after 6 h of reaction (%)	to **2**	to **3**	to **4**	to **5**	to others
HAP	25	23	9	5	59	4
Nb/HAP_i	35	38	2	19	30	11
Nb/HAP_{CW}	33	39	5	10	36	10
Nb/HAP_{CA}	68	22	16	20	29	13

[a]Conditions: toluene solvent; 35 mg cat; 0.66 mmol **1**; 90 °C; batch reactor. [b]Conversion of α-pinene oxide (**1**) after 6 h of TOS. [c]Selectivity under iso-conversion conditions (typically 20%, for all catalysts), to campholenic aldehyde (**2**), carveol (**3**), pinocarveol (**4**), pinocamphone (**5**), and minor compounds (others).

products for all the solids. This suggests that in low polar aprotic solvents (the isomerization tests are run in toluene) the nature of the acid-active sites on this class of materials is mainly of Lewis type.

Then, due to the Nb-hosted in/on HAP structure, catalytic activity of the Nb/HAP samples has been also investigated in reactions involving saccharides (sucrose hydrolysis and glucose isomerization) and in the selective oxidation reactions. For both reactions, many Nb-containing systems have already been recognized as good catalysts.[39,42] In sucrose hydrolysis, when inorganic solid catalysts are considered, the most active sites are associated with Brønsted acid sites. Highly hydrated niobium oxide[48] and niobium phosphate[57] have been recognized as active and selective catalysts for sucrose hydrolysis.

HAP and Nb/HAP samples have been tested in this reaction, performed under mild conditions (80 °C) in aqueous solvent. All the samples are very poorly active (maximum conversion observed ≈1%), indicating the absence of strong Brønsted acid sites on both Nb-free HAP and Nb/HAP samples. The obtained results are presented in Figure 6, in terms of product concentration formed as a function of reaction time. The most acidic sample (in terms of intrinsic and effective acidity, Nb/HAPca) was also the most active one. The order of activity in terms of reaction rate was Nb/HAPca (8.52 $\mu mol_{sucrose} \cdot g^{-1} \cdot h^{-1}$) > HAP (7.54 $\mu mol_{sucrose} \cdot g^{-1} \cdot h^{-1}$) > Nb/HAPcw (5.01 $\mu mol_{sucrose} \cdot g^{-1} \cdot h^{-1}$) > Nb/HAPi (3.46 $\mu mol_{sucrose} \cdot g^{-1} \cdot h^{-1}$).

Glucose isomerization to fructose is a reaction that is typically catalyzed by immobilized enzymes (xylose isomerase) that generates an equilibrium mixture of fructose (42 wt %), glucose (50 wt %), and other saccharides (8 wt %). Basic alkaline-exchanged zeolites and hydrotalcites[58,59] have been proposed as alternative inorganic catalysts for this reaction, and more recently, a solid Lewis acid catalyst in water was proposed by Román-Leshkov et al.[60] Catalysts with amphoteric properties, like HAP and Nb/HAP, are thus expected to show some activity in glucose isomerization. Figure 7 summarizes the

Scheme 1. Acid-Catalyzed Isomerization of α-Pinene Oxide. α-Pinene Oxide (1), Campholenic Aldehyde (2), Carveol (3), Pinocarveol (4) and Pinocamphone (5)

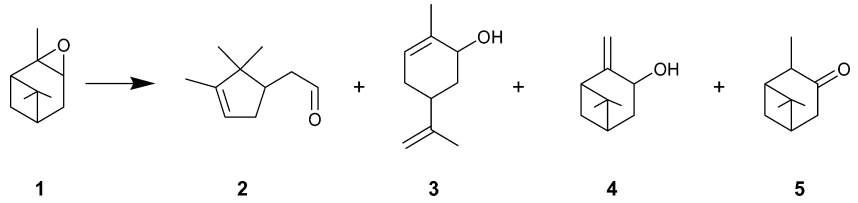

dx.doi.org/10.1021/cs4010453 | ACS Catal. 2014, 4, 469−479

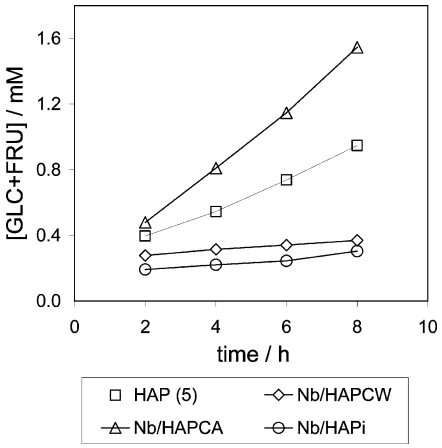

Figure 6. Sucrose hydrolysis reaction: concentration profiles of sucrose and formed products (glucose plus fructose) as a function of reaction time over HAP and Nb/HAP samples (reaction solvent, water; reaction temperature, 80 °C; catalyst mass, ≈0.5 g; sucrose concentration, 0.2 M).

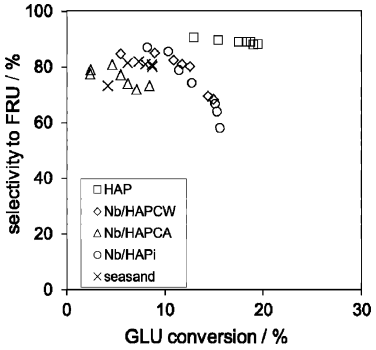

Figure 7. Glucose isomerization reaction: fructose selectivity against glucose conversion over HAP and Nb/HAP samples (reaction solvent, water; reaction temperature, 120 °C; catalyst mass, ≈0.5 g; glucose concentration, 0.55 M).

results obtained on all samples, in terms of fructose selectivity against the glucose conversion. All the catalysts showed high selectivity to fructose at low glucose conversion. At higher conversion, a deactivation trend was observed, in particular on Nb/HAPi and Nb/HAPcw, as already observed in the literature starting from glucose conversion around 15%.[53] On the contrary, bare HAP was able to maintain very high fructose selectivity when glucose conversion increased (above 20%). The order of activity for the catalysts followed the trend: HAP (6.54 $mmol_{glucose}·g^{-1}·h^{-1}$) ≫ Nb/HAPcw (3.83 $mmol_{glucose}·g^{-1}·h^{-1}$) ≃ Nb/HAPi (3.41 $mmol_{glucose}·g^{-1}·h^{-1}$) > Nb/HAPca (1.03 $mmol_{glucose}·g^{-1}·h^{-1}$). A balanced amount of acid and basic sites seems to be necessary to guarantee a good activity, as shown by HAP (I.A./I.B. = 0.71). The remarkable catalytic performances of HAP seems promising and will merit attention in our future experimental activity.

Cyclo-octene epoxidation by aqueous hydrogen peroxide is an oxidation reaction that gives rise to a stable peroxide which does not isomerize easily. For this aim, isolated Nb metal centers show interesting oxidation properties once incorporated in/on inorganic oxide matrices.[18,61] Mesoporous niobiosilicates have been found to be effective catalysts for cyclo-octene epoxidation, and their catalytic activity was found to be strongly influenced by the Nb acid properties and Nb dispersion in the matrix.[24,62] The epoxidation reaction was carried out under mild conditions (55 °C), and at the end of the tests, aqueous hydrogen peroxide was not totally consumed even on the most active catalyst. The calculated reaction rates (calculated at 2 h TOS) are in the following ranking: Nb/HAPcw (1.53 $mmol_{C8}·g^{-1}·min^{-1}$) > Nb/HAPi (1.08 $mmol_{C8}·g^{-1}·min^{-1}$) > Nb/HAPca (0.76 $mmol_{C8}·g^{-1}·min^{-1}$) ≈ HAP (0.72 $mmol_{C8}·g^{-1}·min^{-1}$). As expected, bare HAP was very poorly active and selective. Nb/HAPcw, which has the highest surface area and contained Nb highly dispersed, was the most active sample. In consideration of selectivity to cyclo-octene epoxide, the most acid strength sample, Nb/HAPca, showed the most interesting selectivity (Figure 8).

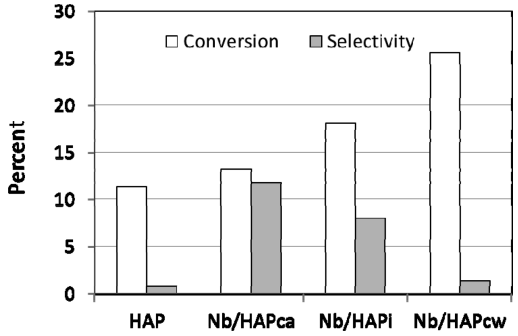

Figure 8. Comparison among samples in the cyclo-octene epoxidation reaction; data have been calculated after 2 h of reaction (reaction solvent, methanol; reaction temperature, 55 °C; catalyst mass, ≈0.6 g; cyclo-octene concentration, 0.45 M, and H_2O_2, 0.45 M.

Analogously, the epoxidation of limonene with aqueous hydrogen peroxide (Scheme 2) was also chosen as a benchmark

Scheme 2. Epoxidation of Limonene to the Limonene Oxide

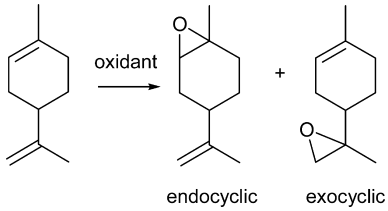

reaction to verify whether Nb(V) sites, in these Nb/HAP solids, are accessible to a bulkier reactant. The catalytic features are reported in Table 5 and in Figure 9, where the selectivity to limonene epoxide is shown as a function of limonene

Table 5. Catalytic Performance of HAP and Nb−HAP Samples in Liquid-Phase Epoxidation of Limonene in the Presence of Aqueous H_2O_2[a]

sample	conversion[b] (%)	yield[c] (%)	conversion[b] (%)	yield[c] (%)
	after 1 h of reaction		after 6 h of reaction	
HAP	12	3	25	10
Nb/HAP_i	29	19	39	24
Nb/HAP_{CW}	19	8	19	8
Nb/HAP_{CA}	20	9	40	7

[a]Conditions: CH_3CN solvent; 100 mg cat; 1.0 mmol limonene; 2.0 mmol aq H_2O_2; reflux temperature; batch reactor. [b]Limonene conversion. [c]Yield to limonene epoxide.

dx.doi.org/10.1021/cs4010453 | ACS Catal. 2014, 4, 469−479

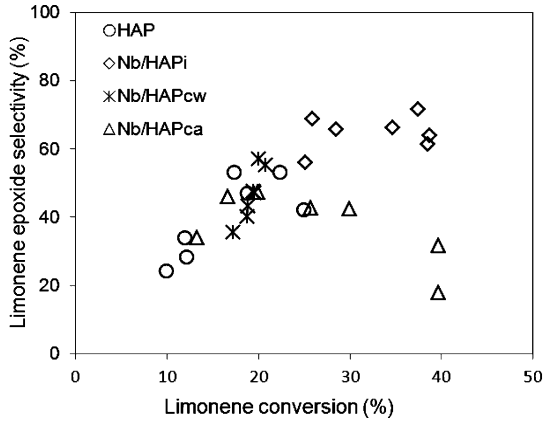

Figure 9. Selectivity vs conversion trend for the liquid-phase epoxidation of limonene over HAP and Nb/HAP samples.

conversion. The role of Nb in promoting the epoxidation reaction was evident, since Nb-free HAP showed the lowest conversion value, after 1 h of reaction, with respect to the other Nb/HAP catalysts. Nevertheless, in this reaction as well, the presence of the niobium centers is not crucial in order to have an effective epoxidation catalyst. Then, Nb/HAPi displayed the most interesting performance, and the results were better, on average, than the ones obtained on the other samples. Over such catalyst, selectivity values as high as ≈70% were obtained at substrate conversion values of ≈40%, with yields in limonene oxide close to 30%. In all cases, however, the (mainly Lewis) acid character of the catalysts was a disadvantage, since the formed epoxide can easily undergo acid-catalyzed ring opening and rearrangement. The epoxide selectivity values were, in fact, poorer than the ones obtained, for instance, over other widely used Nb−silica-based materials on the same substrate. For the sake of comparison, yields in limonene oxide up to 75% can be obtained, under the same conditions, in the presence of grafted Nb−SiO_2 catalysts.[19,20]The formation of undesired secondary products was, in this case, particularly marked for Nb/HAPca, and such behavior is consistent with the observation that Nb/HAPca is the sample with the highest amount of effective acid sites, as from Table 3 and from the direct comparison of the specific activity of the catalysts (Table S.1).

Finally, Nb/HAP catalysts were recovered, thoroughly washed with the fresh solvent, pretreated again, and reused. During the second catalytic run, the initial reaction rate was slower, but then limonene epoxide yields as high as those of the fresh catalyst were attained after 2−4 h of reaction (Figure S.7, SI). In addition, hot-filtration tests have shown no further reaction activity of the solid-free reaction mixture. No leaching of homogeneously active Nb species was thus present.

3. CONCLUDING REMARKS

This study provides the first evidence that Nb centers can be successfully added into (or onto) a hydroxyapatite scaffold. The resulting Nb/HAP samples can be used as a new family of amphoteric catalysts with tunable acid−base properties. The preparation method used for the synthesis affects, to a large extent, the surface properties of the Nb/HAP solids, and it has a major influence, in particular, on the dispersion of niobium species and on the acid to basic sites ratio. Marked differences have been determined between the intrinsic acid properties of the samples and their effective acid properties measured in water that governs the catalytic activity in aqueous solvent. The presence of niobium is mainly associated with Lewis acid sites, which gives a promising catalytic activity not only in acid-promoted isomerization reactions but also in selective oxidation reactions as well, in the presence of aqueous hydrogen peroxide.

The obtained results presented here can open new routes toward the application of this class of solid materials in various reactions of applicative interest.

■ ASSOCIATED CONTENT

Supporting Information

Scheme of the acid sites and basic sites on the HAP matrix; experimental details on thermogravimetric analysis (TGA) of the dried and calcined samples with all the thermograms obtained; SEM and STEM images and EDX maps of calcium, niobium, and phosphorus atom distributions; experimental details on FT-IR spectroscopic analysis with spectra of typical zones of IR absorption; experimental details on UV−vis-DRS analysis with spectra of the samples (Kubelka−Munk function vs energy); experimental details on surface acid and base property determination and data interpretation; experimental details on the reactions of sugars in aqueous solvent (sucrose hydrolysis and glucose isomerization); Table with direct comparison of the specific activity of the catalysts; results of the recovery and reuse of the catalyst in the limonene epoxidation test. This material is available free of charge via the Internet at http://pubs.acs.org.

■ AUTHOR INFORMATION

Corresponding Author

*E-mail: antonella.gervasini@unimi.it. Fax: 0039 02 50314300. Tel.: 0039 02 50314254.

Notes

The authors declare no competing financial interest.

■ ACKNOWLEDGMENTS

All the authors gratefully thank Dr. Matteo Marzo from Dipartimento di Chimica of UNIMI for the experimental support and Dr. Claudio Evangelisti from CNR-ISTM for the HR-TEM analysis. A.G. acknowledges the UCSS de Lille-1, France, Unité de Catalyse et Chimie du Solide, for performing the XPS analyses. C.T. and M.G. acknowledge the Italian Ministry of Education, University and Research through the Project "ItalNanoNet" (Rete Nazionale di Ricerca sulle Nanoscienze; Prot. No. RBPR05JH2P) for economic support.

■ REFERENCES

(1) Elliott, J. C. *Structure and Chemistry of the Apatites and Other Calcium Orthophosphates*; Elsevier: Amsterdam, 1994; Vol. *18*, pp 111−189.
(2) Hench, L. L. *J. Am. Chem. Soc.* **1991**, *74*, 1487−1510.
(3) Lamonier, C.; Lamonier, J.-F.; Aellach, B.; Ezzamarty, A.; Leglise, J. *Catal. Today* **2010**, *164*, 124−130.
(4) Matsumura, Y.; Moffat, J. B. *J. Chem. Soc., Faraday Trans.* **1996**, *92*, 1981−1984.
(5) Dasireddy, V. D. B. C.; Singh, S.; Friedrich, H. B. *Appl. Catal. A: Gen* **2013**, *456*, 105−117.
(6) Tsuchida, T.; Kubo, J.; Yoshihoka, T.; Sakuma, S.; Takeguchi, T.; Ueda, W. *J. Catal.* **2008**, *259*, 183−189.
(7) Aellach, B.; Ezzamarty, A.; Leglise, J.; Lamonier, C.; Lamonier, J.-F. *Catal. Lett.* **2010**, *135*, 197−206.
(8) Wakamura, M.; Kandori, K.; Ishikawa, T. *Colloids Surf., A* **1998**, *142*, 107−116.

(9) Ogo, S.; Onda, A.; Yanagisawa, K. *Appl. Catal. A: Gen* **2011**, *402*, 188−195.
(10) Matsumura, Y.; Moffat, J. B.; Sugiyama, S.; Hayashi, H.; Shigemoto, N.; Soitoli, K. *J. Chem. Soc., Faraday Trans.* **1994**, *90*, 2133−2140.
(11) Wakamura, M.; Kandori, K.; Ishikawa, T. *Colloids Surf., A* **2000**, *164*, 297−305.
(12) Khachani, M.; Kacimi, M.; Ensuque, A.; Piquemal, J. Y.; Connan, C.; Bozon-Verduraz, F.; Ziyad, M. *Appl. Catal. A: Gen* **2010**, *388*, 113−123.
(13) Boucetta, C.; Kacimi, M.; Ensuque, A.; Piquemal, J. Y.; Bozon-Verduraz, F.; Ziyad, M. *Appl. Catal. A: Gen* **2009**, *356*, 201−210.
(14) Ogo, S.; Onda, A.; Yanagisawa, K. *Appl. Catal. A: General* **2008**, *348*, 129−134.
(15) Onda, A.; Ogo, S.; Kajiyoshi, K.; Yanagisawa, K. *Mater. Lett.* **2008**, *62*, 1406−1409.
(16) Ziolek, M. *Catal. Today* **2003**, *78*, 47−64.
(17) Wachs, I. E.; Jehng, J.-M.; Deo, G.; Arora, N. *Catal. Today* **1996**, *28*, 199−205.
(18) Lacerda, V., Jr.; Araujo dos Santos, D.; da Silva-Filho, L. C.; Greco, S. J.; Bezerra dos Santos, R. *Adrichim. Acta* **2012**, *45*, 19−27.
(19) Gallo, A.; Tiozzo, C.; Psaro, R.; Carniato, F.; Guidotti, M. *J. Catal.* **2012**, *298*, 77−83.
(20) Tiozzo, C.; Bisio, C.; Carniato, F.; Gallo, A.; Scott, S. L.; Psaro, R.; Guidotti, M. *Phys. Chem. Chem. Phys.* **2013**, *15*, 13354−13362.
(21) Guerrero-Pérez, M. O.; Bañares, M. A. *Catal. Today* **2009**, *142*, 243−251.
(22) Trejda, M.; Kujawa, J.; Ziolek, M.; Mrowiec-Bialón, J. *Catal. Today* **2008**, *139*, 196−201.
(23) Coelho, J. V.; Oliveira, L. C. A.; Moura, F. C. C.; de Souza, P. P.; Silva, C. A.; Batista, K. B.; Silva, M. J. *Appl. Catal. A: Gen* **2012**, *419*−*420*, 215−220.
(24) Aronne, A.; Turco, M.; Bagnasco, G.; Ramis, G.; Santacesaria, E.; Di Serio, M.; Marenna, E.; Bevilacqua, M.; Cammarano, C.; Fanelli, E. *Appl. Catal. A: Gen* **2008**, *347*, 179−185.
(25) Carniti, P.; Gervasini, A.; Marzo, M. *J. Phys. Chem. C* **2008**, *112*, 14064−14074.
(26) Gao, X.; Wachs, I. E.; Wong, M. S.; Ying, J. Y. J. *Catal* **2001**, *203*, 18−24.
(27) Ziolek, M.; Sobczak, I.; Lewandowska, A.; Nowak, I.; Decyk, P.; Renn, M.; Janowska. *Catal. Today* **2001**, *70*, 169−181.
(28) Corma, A.; Llabrés i Xamena, X.; Prestipino, C.; Renz, M.; Valencia, S. *J. Phys. Chem. C* **2009**, *113*, 11306−11315.
(29) Tanaka, M.; Shima, H.; Yokoi, T.; Tatsumi, T.; Kondo, J. N. *Catal. Lett.* **2011**, *141*, 283−292.
(30) Hävecker, M.; Wrabetz, S.; Kröhnert, J.; Csepei, L.-I.; Nauman d'Alnoncourt, R.; Kolen'ko, Y. V.; Girgsdies, F.; Schlögl, R.; Trunschke, A. *J. Catal.* **2012**, *285*, 48−60.
(31) Roussel, M.; Bouchard, M.; Bordes-Richard, E.; Karim, K.; Al-Sayari, S. *Catal. Today* **2005**, *99*, 77−87.
(32) Glaum, R.; Welker-Nieuwoudt, C.; Dobner, C. K.; Eichelbaum, M.; Gruchow, F.; Heine, C.; Karpov, A.; Kniep, R.; Rosowski, F.; Schlögl, R.; Schunk, S. A.; Titlbach, S.; Trunschke, A. *Chem. Ing. Tech.* **2012**, *84*, 1766−1779.
(33) Nguyen, T. T.; Aouine, M.; Millet, J. M. M. *Catal. Commun.* **2012**, *21*, 22−26.
(34) Dibenedetto, A.; Aresta, M.; Angelini, A.; Ethiraj, J.; Aresta, B. M. *Chem.—Eur. J.* **2012**, *18*, 10324−10334.
(35) Okumura, K.; Tomiyama, T.; Shirakawa, S.; Ishida, S.; Sanada, T.; Arao, M.; Niwa, M. *J. Mater. Chem.* **2011**, *21*, 229−235.
(36) de La Cruz, M. H. C.; Rocha, M. S.; Lachter, E. R.; Forrester, A. M. S.; Reis, M. C.; San Gil, R. A. S.; Caldarelli, S.; Farias, A. D.; Gonzalez, W. A. *Appl. Catal. A: Gen* **2010**, *386*, 60−64.
(37) Okuhara, T. *Chem. Rev.* **2002**, *102*, 3641−3666.
(38) Nakaijma, K.; Baba, Y.; Noma, R.; Kitano, M.; Kondo, J. N.; Hayashi, S.; Hara, M. *J. Am. Chem. Soc.* **2011**, *133*, 4224−4227.
(39) Carniti, P.; Gervasini, A.; Biella, S.; Auroux, A. *Chem. Mater.* **2005**, *17*, 6128−6136.
(40) Carniti, P.; Gervasini, A.; Biella, S.; Auroux, A. *Catal. Today* **2006**, *118*, 373−378.
(41) Carniti, P.; Gervasini, A.; Marzo, M. *Catal. Today* **2010**, *152*, 42−47.
(42) Gervasini, A.; Carniti, P.; Marzo, M.; Auroux, A. *J. Catal.* **2012**, *296*, 143−155.
(43) Landi, E.; Tampieri, A.; Celotti, G.; Sprio, S. *J. Eur. Ceram. Soc.* **2000**, *20*, 2377−2387.
(44) Bernache-Assolant, D.; Ababoua, A.; Champion, E.; Heughebaert, M. *J. Eur. Ceram. Soc.* **2003**, *23*, 229−241.
(45) Lazić, S.; Zec, S.; Miljević, N.; Milonjić, S. *Thermochim. Acta* **2001**, *374*, 13−22.
(46) Suguyama, S.; Hayashi, H. *Int. J. Mod. Phys. B* **2003**, *17*, 1476−1481.
(47) Zhu, H.; Zheng, Z.; Gao, X.; Huang, Y.; Yan, Z.; Zou, J.; Yin, H.; Zou, Q.; Kable, S. H.; Zhao, J.; Xi, Y.; Martens, W. N.; Frost, R. L. *J. Am. Chem. Soc.* **2006**, *128*, 2373−2384.
(48) Sumiya, S.; Oumi, Y.; Sadakane, M.; Sano, T. *Appl. Catal. A: Gen* **2009**, *365*, 261−267.
(49) Dragone, L.; Moggi, P.; Predieri, G.; Zanoni, R. *Appl. Surf. Sci.* **2002**, *187*, 82−88.
(50) Carniti, P.; Gervasini, A.; Marzo, M.; Auroux, A. *Thermochim. Acta* **2013**, *567*, 51−56.
(51) Marzo, M.; Gervasini, A.; Carniti, P. *Catal. Today* **2012**, *192*, 89−95.
(52) Kaminska, J.; Schwegler, M. A.; Hoefnagel, A. J.; van Bekkum, H. *Recl. Trav. Chim. Pays-Bas* **1992**, *111*, 432−437.
(53) Wilson, K.; Renson, A.; Clark, J. H. *Catal. Lett.* **1999**, *61*, 51−55.
(54) Ravindra, D. B.; Nie, Y. T.; Jaenicke, S.; Chuah, G. K. *Catal. Today* **2004**, *96*, 147−153.
(55) Ravasio, N.; Zaccheria, F.; Guidotti, M.; Psaro, R. *Topics Catal.* **2004**, *27*, 157−168.
(56) Ostinelli, L.; Recchia, S.; Bisio, C.; Carniato, F.; Guidotti, M.; Marchese, L.; Psaro, R. *Chem. Asian J.* **2012**, *7*, 2394−2402.
(57) Marzo, M.; Gervasini, A.; Carniti, P. *Carbohydr. Res.* **2012**, *347*, 23−31.
(58) Moreau, C.; Durand, R.; Roux, A.; Tichit, D. *Appl. Catal. A: Gen* **2000**, *193*, 237−264.
(59) Lecomte, J.; Finiels, A.; Moreau, C. *Starch/Stärke* **2002**, *54*, 75−79.
(60) Román-Leshkov, Y.; Moliner, M.; Labinger, J. A.; Davis, M. E. *Angew. Chem., Int. Ed.* **2010**, *49*, 8954−8957.
(61) Nowak, I.; Ziolek, M. *Chem. Rev.* **1999**, *99*, 3603−3624.
(62) Gallo, J. M. R.; Paulino, I. S.; Schuchardt, U. *Appl. Catal. A: Gen* **2004**, *266*, 223−227.